

## ORIGINAL ARTICLE

# Regression analysis and features of negative activation energy for MHD nanofluid flow model: A comparative study



B. Kumar<sup>a,\*</sup>, Prachi<sup>b</sup>, Abhinav Singhal<sup>c</sup>, R. Nandkeolyar<sup>d</sup>, Pulkit Kumar<sup>e</sup>, Ali J. Chamkha<sup>f</sup>

<sup>a</sup>School of Mathematics, Thapar Institute of Engineering and Technology, Patiala 147004, Punjab, India

<sup>b</sup>Department of Applied Sciences and Humanities, RIT, Roorkee 247667, India

<sup>c</sup>School of Sciences, Christ (Deemed to be University), Delhi NCR 201003, India

<sup>d</sup>Department of Mathematics, National Institute of Technology, Jamshedpur 831014, India

<sup>e</sup>Department of Applied Mechanics, Indian Institute of Technology, Delhi 110016, India

<sup>f</sup>Faculty of Engineering, Kuwait College of Science and Technology, Doha District, Kuwait

Received 4 December 2021; accepted 10 December 2022

Available online 10 April 2023

## KEYWORDS

Negative activation energy;  
Regression analysis;  
Successive linearization method;  
Porous medium

**Abstract** This article elucidates the impact of activation energy on magnetohydrodynamic (MHD) stagnation point nanofluid flow over a slippery surface in a porous regime with thermophoretic and Brownian diffusions. Negative activation energy is scarce in practice, but the impact of negative activation energy could not be neglected as it is noticed in chemical processes. The rate of some Arrhenius-compliant reactions is retarded by increasing the temperature and is therefore associated with negative activation energies, such as exothermic binding of urea or water. In some processes, the temperature dependence of the pressure-induced unfolding and the urea-induced unfolding of proteins at ambient pressure give negative activation energies. The present mathematical model is solved with successive linearization method (a spectral technique). A comparison of results is made for negative and positive values of activation energy. Apart from it, the quadratic multiple regression model is discussed briefly and explained with bar diagrams. It is observed that with rise in unsteadiness parameter from

\*Corresponding author.

E-mail address: [chauhanbhuvan6@gmail.com](mailto:chauhanbhuvan6@gmail.com) (B. Kumar).

Peer review under responsibility of Propulsion and Power Research.



<https://doi.org/10.1016/j.jprr.2023.02.005>

2212-540X/© 2023 The Authors. Publishing services by Elsevier B.V. on behalf of KeAi Communications Co. Ltd. This is an open access article under the CC BY-NC-ND license (<http://creativecommons.org/licenses/by-nc-nd/4.0/>).

0 to 1 (taking positive activation energy), skin friction and Sherwood number are increased by 9.36% and 19% respectively, and Nusselt number is decreased by 26%. However, for negative activation energy, 9.36% and 112% enhancement is observed in skin friction and Sherwood number, respectively.

© 2023 The Authors. Publishing services by Elsevier B.V. on behalf of KeAi Communications Co. Ltd. This is an open access article under the CC BY-NC-ND license (<http://creativecommons.org/licenses/by-nc-nd/4.0/>).

## Nomenclature

$a, b$	arbitrary constants	$Pr$	Prandtl number
$B$	magnetic field (unit: T)	$q_w$	heat flux at the surface (unit: $W \cdot m^{-2}$ )
$\phi$	nanoparticle volume fraction (unit: $kg/m^3$ )	$Re_x$	local Reynolds number
$Cf_x$	skin friction coefficient	$r$	stagnation parameter
$\phi_\infty$	ambient species concentration (unit: $kg/m^3$ )	$R$	radiation parameter
$c_p$	specific heat at a constant pressure (unit: $J \cdot kg^{-1} \cdot K^{-1}$ )	$T$	fluid temperature (unit: K)
$D_B$	coefficient of Brownian diffusion	$T_w$	fluid temperature at stretching sheet (unit: K)
$D_T$	coefficient of thermos-phoretic diffusion	$T_\infty$	ambient fluid temperature (unit: K)
$E_a$	activation energy (unit: J)	$u$	velocity in the $x$ direction (unit: $m \cdot s^{-1}$ )
$f$	stream function	$u_w$	stretching velocity (unit: $m \cdot s^{-1}$ )
$g$	gravitational acceleration (unit: $m \cdot s^{-2}$ )	$u_\infty$	free stream fluid velocity (unit: $m \cdot s^{-1}$ )
$k$	thermal conductivity (unit: $W \cdot m^{-1} \cdot K^{-1}$ )	$v$	fluid velocity in the $y$ direction (unit: $m \cdot s^{-1}$ )
$k_0$	porous permeability	$x, y$	coordinate directions (unit: m)
$k_B$	Boltzmann constant	$\theta(\eta)$	dimensionless temperature
$K$	porous permeability parameter	$\mu$	dynamic viscosity (unit: $kg \cdot m^{-1} \cdot s^{-1}$ )
$Sc$	Schmidt number	$\nu$	kinematic viscosity (unit: $m^2 \cdot s^{-1}$ )
$M$	magnetic parameter	$(\rho c)_f$	nanofluid heat capacity
$Nb$	Brownian motion parameter	$(\rho c)_p$	nanoparticles heat capacity
$Nt$	thermos-phoretic parameter	$\sigma^*$	electric conductivity (unit: $S \cdot m^{-1}$ )
$Nu_x$	local Nusselt number	$\tau_w$	surface shear stress (unit: $N \cdot m^{-2}$ )
		$s(\eta)$	dimensionless concentration

## 1. Introduction

A nanofluid is a fluid having nanometre-sized particles called nanoparticles. The main goal of nanofluids is to achieve the highest possible thermal properties at the smallest possible concentrations by uniform dispersion and stable suspension of nanoparticles in host fluids. These fluids are engineered colloidal suspensions of nanoparticles in a base fluid. The nanoparticles used in nanofluids are typically made of metals, oxides, carbides, or carbon nanotubes. Common base fluids include water, ethylene glycol and oil. The nano-scale particles which are utilized in these sorts of fluids are generally made of oxides, carbides, and metals. Nanofluid plays an essential part in numerous fields, for example, chemical science, environmental science, electronics, nuclear system, industries, and medical science etc. Some useful and innovative study on nanofluid is presented by several authors viz [1–3]. Sheikholeslami and Farshad [4] has scrutinized flat plate solar collector with employing hybrid nanomaterial. Turbulent flow within the pipe was modeled by Sheikholeslami et al. [5]. Some other interesting model based on nanofluid flow was studied by

Sheikholeslami [6,7]. Haque et al. [8] provided a review on laminar forced convection heat transfer of nanofluids. This review also offers details on the most widely used correlations used to predict the efficient thermophysical properties of nanofluids. Ebrahimmataj et al. [9] studied the effect of soot accumulation and backpressure of an integrated after-treatment system on diesel engine performance. Hadi and Ali [10] studied super hydrophobic wavy mini channel heat sink for thermal and hydraulic analysis using  $SiO_2$  and  $TiO_2$  aqueous nanofluids. Purree et al. [11] have written a brief review on synthesis, heat transfer properties and stability of nanofluids for commercialization. Articles based on the stagnation point flow of nanofluid are reported in the literature [12,13].

The relationship between temperature and the reaction rate is incorporated by Arrhenius [14]. Activation energy is the minimum amount of energy that must provide to compounds to result in a chemical reaction. The Arrhenius equation allows us to calculate activation energies if the rate constant is known, or vice versa. The activation energy for a reaction is sometimes measured under different reaction conditions. An example might be a measurement using a

very active catalyst at a moderate temperature and a less active catalyst at higher temperatures. The increase in temperature partially compensates for the lower activity. Contrary to expectations of equal activation energy, however, different activation energies and different pre-exponential factors are found. The Arrhenius activation energy is experimentally determined, and it is related to threshold energies and the success of individual collisions at the molecular level.

The development of mass transfer phenomena with chemical reactions has attracted substantial interest to the researcher and scientists because of its numerous valuable applications in oil reservoir, chemical engineering, nuclear reactor cooling, geothermal engineering, deterioration of materials, mechanochemistry, oil and water emulsions. Usually the relation of chemical reactions with mass transfer is very complicated, it can be regularly examined through fabrication and digestion of reactant species at dissimilar rates for both within the mass transfer and fluid flow. The terminology of activation energy was initially proposed by Arrhenius [14]. Javed et al. [15] studied melting heat transfer along with binary chemical reaction and activation energy in stagnation flow over a sheet of variable thickness saturated in a porous medium. It is observed that the concentration field gets intensified for larger values of the activation energy parameter, and the velocity field decreases for larger porosity parameter. Majeed et al. [16] examined unsteady gyrotactic microorganism bioconvective magnetohydrodynamic flow toward a stretchable surface under the impact of thermal radiation with activation energy. Saleem et al. [17] have performed thermal analysis of double diffusive electrokinetic thermally radiated  $\text{TiO}_2\text{-Ag}$ /blood stream triggered by synthetic cilia under buoyancy forces and activation energy. The analysis reveals that the elevated electric potential and prolonged cilia assist directional flow spreads over large distances. Some other related studies are reported in the articles [18–20].

The negative value of activation energy is real in very few cases. Negative activation energy is possible even for elementary reactions [21]. In these cases, there are attractive forces between reactants, there are no barrier, or the barrier is submerged. In some cases, (eg. the reaction of ionic species), there are no barrier that result in negative activation energy.

In the present article, we have analysed magnetohydrodynamic (MHD) stagnation point flow of nanofluid over a slippery surface in a porous regime by taking both positive and negative values of activation energy, thermal radiation, thermophoretic and Brownian diffusions. The model is solved by successive linearization method. Several models are available on stagnation point flow of fluid but the novelty of our model is that we have focused on the features of negative and positive activation energy on a nanofluid flow model by considering the effects of velocity slip, thermal radiation, thermophoretic and Brownian diffusions. The model is solved by spectral technique. Moreover, regression model is presented by considering thermophoretic and

Brownian diffusion parameter as a function of Sherwood number. As per the author's concern, this model is not discussed so far.

## 2. Mathematical formulation

We have considered two-dimensional, incompressible, laminar, hydromagnetic, viscous and electrically conducting, heat radiating nanofluid flow over a stretching sheet in a porous medium with chemical reaction. Cu-water nanofluid is considered for calculations, here water is base fluid.  $O$  is the stagnation point at which local velocity of fluid is zero.  $x$  and  $y$  are the coordinate axes which are chosen in such a way that  $x$ -axis corresponds to the distance along the sheet, however,  $y$ -axis corresponds the distance normal to the sheet (see Figures 1 and 2). It is also assumed that nanofluid is impinging normally over sheet. Free stream velocity and stretching sheet velocity are time dependent that is assumed as  $u_\infty(x, t) = \frac{bx}{(1-\lambda t)}$ ,  $u_w(x, t) = \frac{ax}{(1-\lambda t)}$

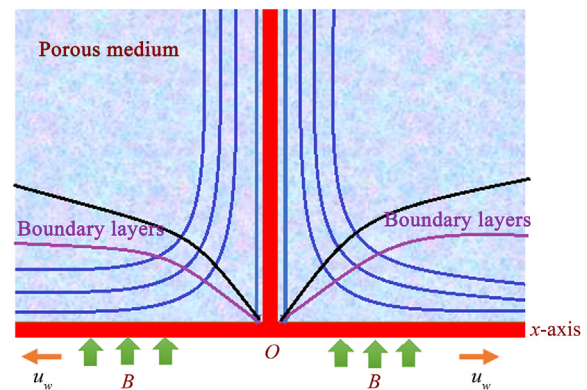


Figure 1 Geometry of the model.

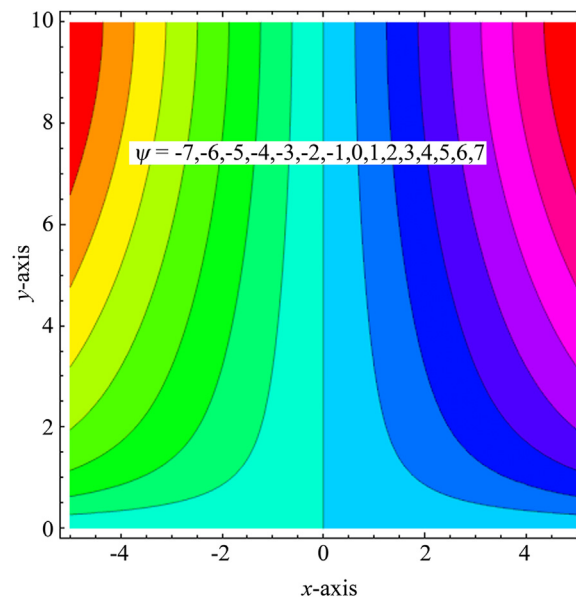


Figure 2 Streamlines of the flow.

respectively. Here  $a, b$  and  $\lambda$  are constants and the dimension of  $\lambda$  is reciprocal of time. A magnetic field of intensity  $B(x, t)$  is applied normal to  $x$ -axis. Induced magnetic field is neglected. The governing equations [22–24] are:

$$\frac{\partial u}{\partial x} + \frac{\partial v}{\partial y} = 0, \tag{1}$$

$$u \frac{\partial u}{\partial x} + v \frac{\partial u}{\partial y} + \frac{\partial u}{\partial t} = \nu \frac{\partial^2 u}{\partial y^2} + \frac{\partial u_\infty}{\partial t} + u_\infty \frac{du_\infty}{dx} - \frac{\sigma^* B^2 (u - u_\infty)}{\rho_f} - \frac{v(u - u_\infty)}{k_0}, \tag{2}$$

$$u \frac{\partial T}{\partial x} + v \frac{\partial T}{\partial y} + \frac{\partial T}{\partial t} = \alpha_m \frac{\partial^2 T}{\partial y^2} + \frac{1}{(\rho c)_f} \frac{16\sigma^{**} T_\infty^3}{3k^*} \frac{\partial^2 T}{\partial y^2} + \tau \left[ \frac{D_T}{T_\infty} \left( \frac{\partial T}{\partial y} \right)^2 + D_B \frac{\partial \phi}{\partial y} \frac{\partial T}{\partial y} \right], \tag{3}$$

$$u \frac{\partial \phi}{\partial x} + v \frac{\partial \phi}{\partial y} + \frac{\partial \phi}{\partial t} = \frac{D_T}{T_\infty} \frac{\partial^2 T}{\partial y^2} + D_B \frac{\partial^2 \phi}{\partial y^2} - k_r^2 (\phi - \phi_\infty) \left( \frac{T}{T_\infty} \right)^m \exp \left( \frac{-E_a}{k_B T} \right). \tag{4}$$

Related boundary conditions are:

$$t \leq 0 : T = T_w, \phi = \phi, u(x, t) = 0, v(x, t) = 0,$$

For  $t > 0$ , at  $y = 0$ ,

$$T = T_w, \phi = \phi_w, u = u_{slip} + u_w = \frac{N\mu\partial u}{\partial y} + u_w, v = 0$$

as  $y \rightarrow \infty$

$$T \rightarrow T_\infty, \phi \rightarrow \phi_\infty, u \rightarrow u_\infty$$

The meaning of symbols is given in nomenclature section.

The similarity transformation [1] is given by:

$$\left. \begin{aligned} \psi &= \sqrt{uxu_w(x, t)} f(\eta), \eta = y \sqrt{\frac{u_w(x, t)}{ux}}, \\ s(\eta) &= \frac{\phi - \phi_\infty}{\phi_w - \phi_\infty}, \theta(\eta) = \frac{T - T_\infty}{T_w - T_\infty}. \end{aligned} \right\}$$

Here  $\psi$  is a stream function which is defined as  $(u, v) = \left( \frac{\partial \psi}{\partial y}, -\frac{\partial \psi}{\partial x} \right)$ . Here  $f(\eta)$  is a dimensionless stream function,  $\eta$  is similarity variable,  $s(\eta)$  is dimensionless nanoparticle concentration and  $\theta(\eta)$  is non-dimensional temperature. For obtaining the similar solution, we have taken time dependent variable transverse magnetic field  $B(x, t) = \frac{B_0}{\sqrt{(1-\lambda t)}} (B_0 \neq 0)$ , time dependent porous permeability  $k_0 = k_p(1-\lambda t)$  and velocity slip factor  $N = N_1 \left( \frac{1}{(1-\lambda t)} \right)^{-1/2}$ .

Where  $B_0, k_p$  and  $N_1$  are the constant magnetic field, porous permeability and initial velocity slip factor, respectively.

Using similarity transformation in Eqs. (2)–(4), we get-

$$f''' - f'^2 + ff'' - (M + K)(f' - r) - A \left( f' + \frac{\eta}{2} f'' - r \right) + r^2 = 0, \tag{5}$$

$$1/Pr_{eff} \theta'' + Nbs' \theta' + f \theta' + Nt \theta^2 - \frac{A}{2} \eta \theta' = 0, \tag{6}$$

$$s'' + Scfs' + Sc\sigma^* (1 + \delta \theta)^m s \exp \left( -\frac{E}{1 + \delta \theta} \right) - \frac{A Sc}{2} \eta s' + \frac{Nt}{Nb} \theta'' = 0, \tag{7}$$

Transformed boundary constraints are:

at  $\eta = 0$ :

$$\theta(\eta) = 1, s(\eta) = 1, f(\eta) = 0, f'(\eta) = \gamma f''(\eta)$$

$$\text{as } \eta \rightarrow \infty : \theta(\eta) \rightarrow 0, s(\eta) \rightarrow 0, f'(\eta) \rightarrow r \tag{8}$$

Where  $r = \frac{b}{a}, M = \frac{\sigma^* B_0^2}{\rho_f a}, K = \frac{\nu}{ak_p}, A = \frac{\lambda}{a}, Pr = \frac{\nu}{\alpha}, Pr_{eff} = \frac{Pr}{(1+R)}, R = \frac{16T_\infty^3 \sigma^{**}}{3kk^*}, Nt = \frac{\tau D_T (T_w - T_\infty)}{T_\infty \nu}, Nb = \frac{\tau D_B (\phi_w - \phi_\infty)}{\nu}, \gamma = N_1 \rho_f (a\nu)^{1/2}, \delta = \frac{(T_w - T_\infty)}{T_\infty}, E = \frac{E_a}{k_B T_\infty}, \sigma = \frac{k^2}{a}$ , and  $Sc = \frac{\nu}{D_B}$  are the stagnation parameter, magnetic parameter, porous permeability parameter, unsteadiness parameter, Prandtl number, effective Prandtl number, radiation parameter, thermophoretic parameter, Brownian motion parameter, velocity slip parameter, temperature difference parameter, non-dimensional activation energy, dimensionless chemical reaction parameter and Schmidt number respectively.

The local Nusselt number  $Nu_x$  [1,24], local skin friction coefficient  $Cf_x$  [24,25], and the local Sherwood number  $Sh_x$  are defined as follows-

$$Cf_x = \frac{\tau_w}{\rho u_w^2(x, t)}, Nu_x = \frac{xq_w}{k(T_w - T_\infty)}$$

$$Sh_x = \frac{xq_m}{D_B(\phi_w - \phi_\infty)}$$

where  $q_w$  [26],  $\tau_w$  and  $m_w$  are the surface heat flux, shear stress, and mass flux respectively which are defined as:

$$\tau_w = \mu \left( \frac{\partial u}{\partial y} \right)_{y=0}, q_w = - \left[ \left( k + \frac{16\sigma T^3}{3k^*} \right) \frac{\partial T}{\partial y} \right]_{y=0},$$

$$m_w = -D_B \left( \frac{\partial \phi}{\partial y} \right)_{y=0}$$

After using similarity transform, we get following form of these physical quantities-

$$\begin{aligned} Cf_x Re_x^{1/2} &= f''(0), Nu_x Re_x^{-1/2} = -(1 + R)\theta'(0), \\ Sh_x Re_x^{-1/2} &= -s'(0) \end{aligned}$$

Where  $Re_x$  is the local Reynold number.

### 3. Solution methodology

SLM technique [27] is used to solve non linear ODEs Eqs. (5)–(7) along with the boundary conditions written in Eq. (8). Spectral methods take on a global approach to deal with the problem, i.e. the value of a derivative at a certain point in space depends on the solution at all the other points in space, and not just the neighbouring grid points. For this reason, spectral methods have excellent error properties with the so called exponential convergence being the fastest possible, when the solution is smooth. Spectral methods are distinguished not only by the fundamental type of the method (Galerkin collocation, Galerkin with numerical integration), but also by the particular choice of the trial functions. Due to this fact, spectral methods usually have a very high order of approximation. In fact, spectral methods were among the first to be used in practical flow simulations. The details of convergence analysis of spectral methods is available in books [28,29].

For utilizing this technique, the functions  $f(\eta)$ ,  $\theta(\eta)$  and  $s(\eta)$  are considered as:

$$\left. \begin{aligned} f(\eta) &= f_j(\eta) + \sum_{w=0}^{j-1} F_w(\eta), \\ \theta(\eta) &= \theta_j(\eta) + \sum_{w=0}^{j-1} \Theta_w(\eta), \\ s(\eta) &= s_j(\eta) + \sum_{w=0}^{j-1} W_w(\eta), \end{aligned} \right\} \quad (9)$$

Where  $F_w(\eta)$ ,  $\Theta_w(\eta)$  and  $W_w(\eta)$  are successive approximation while functions  $f(\eta)$ ,  $\theta(\eta)$  and  $s(\eta)$  are unknown which can be obtained by solving linear part of obtained system of equation. We have to choose initial guess that satisfy boundary conditions. Let the initial guesses are i.e.

$$\left. \begin{aligned} F_0(\eta) &= r\eta + \frac{1-r}{1+\gamma}(1 - e^{-\eta}), \\ \Theta_0(\eta) &= e^{-\eta}, W_0(\eta) = -e^{-\eta}. \end{aligned} \right\}$$

Substituting Eq. (9) in to Eqs. (5)–(8), we obtain linearize form of system of equations. Solving these linearized equations and using initial guesses, we get the corresponding solutions. The solutions of  $f(\eta)$ ,  $\theta(\eta)$  and  $s(\eta)$  after  $n$  iterations can be expressed as:

$$\left. \begin{aligned} f(\eta) &\approx \sum_{w=0}^M F_w(\eta), \theta(\eta) \approx \sum_{w=0}^M \Theta_w(\eta), \\ s(\eta) &\approx \sum_{w=0}^M W_w(\eta). \end{aligned} \right\}$$

These linearized equations are solved by using Chebyshev spectral collocation scheme in which polynomials are defined on  $[-1, 1]$  closed interval. By using domain truncation method, the domain  $[0, \infty)$  is converted to  $[-1, 1]$ .

Let  $P$  be the number of collocation points and Gauss-Lobatto collocation points method is used to discretize the domain  $[-1, 1]$ , which is defined as follows:

$$\frac{\eta}{L^*} = \frac{\zeta + 1}{2}, -1 \leq \zeta \leq 1.$$

At these  $P$  collocation points, the functions  $F_j$ ,  $\Theta_j$  and  $W_j$  for  $j \geq 1$  are approximated with the help of  $k^{th}$  Chebyshev polynomial and then we calculate the  $r^{th}$  derivative of functions at the collocation points. In this procedure, we get following matrix equation:

$$A_{j-1} X_j = R_{j-1}.$$

Where  $A_{j-1}$  is a  $(4P+4) \times (4P+4)$  square matrix,  $X_j$  and  $R_{j-1}$  are  $(4P+4) \times 1$  column vectors. This matrix system is solved in MATLAB software.

### 4. Validation of solution

In order to justify our results, we have carried out a comparison in limiting sense between our results and results obtained by Khan and Pop [30]. Good agreement between them can be seen from Table 1 that leads to justify the present results.

**Table 1** Validation table.

$Nb$	$Nt$	Khan and Pop [30] $\theta'(0)$	Present $\theta'(0)$ [30]	Khan and Pop $s'(0)$	Present $s'(0)$
0.1	0.1	0.9524	0.9521	2.1294	2.1291
0.1	0.2	0.6932	0.6932	2.2740	2.2740
0.1	0.3	0.5201	0.5203	2.5286	2.5282
0.2	0.1	0.5056	0.5053	2.3819	2.3816
	0.2	0.3654	0.3651	2.5152	2.5151
	0.3	0.2731	0.2732	2.6555	2.6557

### 5. Results and discussion

The present analysis deals with stagnation point flow of nanofluid over a slippery surface embedded in a porous medium. We have plotted velocity, temperature and concentration profiles for flow controlling parameters. For numerical computation, we have taken  $M = 0.5$ ,  $A = 1$ ,  $K = 0.5$ ,  $Pr = 6.7$ ,  $Sc = 2$ ,  $Nb = 0.2$ ,  $\delta = 0.9$ ,  $\sigma = 0.5$ ,

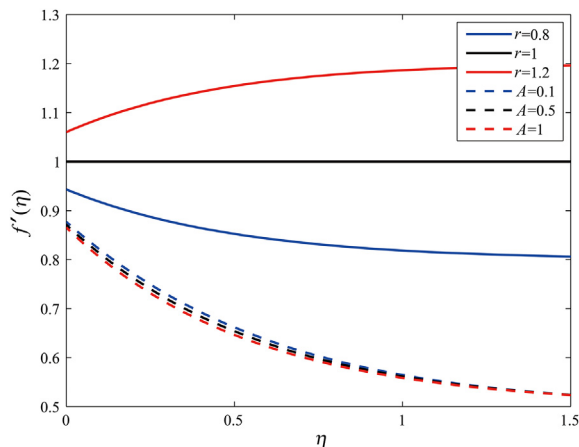


**Figure 3** Variation of fluid velocity ( $f'(\eta)$ ) with parameters  $r$  and  $A$ .

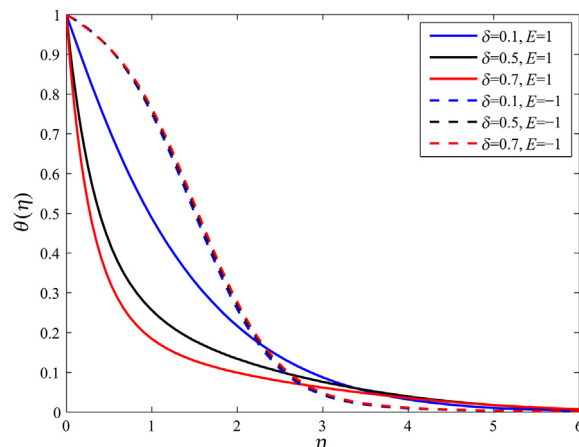


**Figure 4** Variation of fluid temperature with parameters  $\delta$  and  $E$ .

$E = 1, Nt = 0.2, r = 0.5, R = 1$  and  $\gamma = 0.2$  as a default value, until otherwise specified particularly.

Figure 3 is plotted to observe the effect of parameters  $A$  and  $r$  on the flow field. It is noticed here that for  $r = 1$ , no boundary layer is formed because free stream and stretching sheet velocities are same. Also, the boundary layers for  $r < 1$  is exactly the mirror image of the boundary layer for  $r > 1$ . The reason behind this behaviour is pretty apparent by the definition of stagnation parameter.  $r < 1$  indicates that the free stream is moving faster than the stretching sheet, and  $r > 1$  represents conversely. Therefore, boundary layers get reversed in these cases. In the same figure, the impact of parameter  $A$  is observed. It can be seen that, for the chosen value of  $A$ , all curves merge to 0.5, because the boundary conditions we have chosen are in such a way that velocity should merge to  $r$  as  $\eta$  tends to infinity and the default value of  $r$  is 0.5. Further, the parameter  $A$  causes a reduction in the velocity profile because rate of stretching velocity is decreased with parameter  $A$ . A significant contribution of activation energy on fluid velocity is not noticed, therefore, the velocity profiles corresponding to activation energy are not drawn.

Figure 4 captures the behaviour of temperature of fluid with parameters  $\delta$  and  $E$ . Two different styles of lines are plotted, the plane line represents graphs for  $E = 1$  and dotted lines for  $E = -1$ . Parameter  $\delta$  amplifies the temperature for  $E = -1$  and exactly opposite behaviour is observed for  $E = 1$ . The reason behind this variation can be described by the definition of parameter  $\delta$ . The difference in temperature of the wall and away from the wall increases with enhancement in the parameter  $\delta$ ; therefore, free stream temperature declines to manage it. Apart from opposite behaviour of  $\delta$  in these cases, the boundary layer gets thinner in the case of  $E = -1$ . In a similar pattern, Figure 5 is displayed for concentration profile. It is interesting to note that parameter  $\delta$  boosts the temperature profile up for  $E = 1$

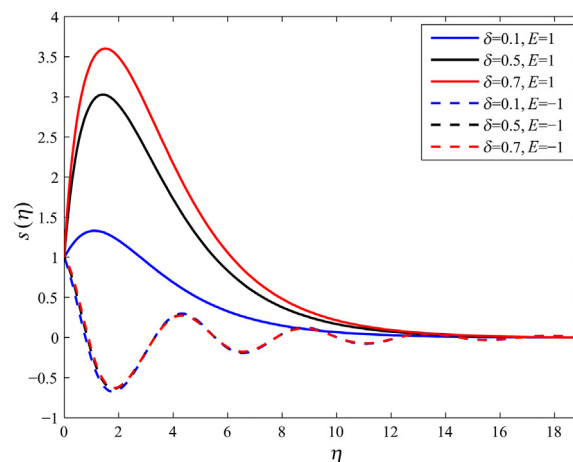


**Figure 5** Variation of fluid concentration with parameters  $\delta$  and  $E$ .

and the maximum concentration is found when  $\eta$  is around 2. For negative value of  $E$ , wavy concentration curve is obtained and the curve has multiple zeroes. Here the physical meaning of zeroes relates to the fact that fluid achieves free stream concentration at some points within the boundary layer. This result does not sound good and looks unexpected but the fact that we have taken negative activation energy into account could not be ignored.

The temperature and concentration profiles for parameter  $E$  is displayed in Figures 6 and 7. At a given temperature, the activation energy depends on the nature of the chemical transformation that takes place, but not on the relative energy state of the reactants and products. Figure 6 indicates that temperature goes up with enhancement in  $E$ , also the behaviour is same for both positive and negative values of  $E$ . For  $E = 2$ , a hump in temperature profile is found, which is maximum when  $\eta = 1.8$ . The boundary layer gets thinner for negative  $E$  values. Figure 7 suggests that the concentration profile declines with positive  $E$  values. The wavy

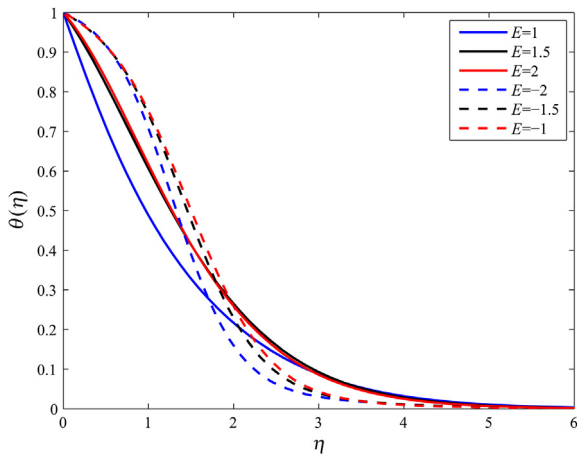


**Figure 6** Variation of fluid temperature with parameter  $E$ .

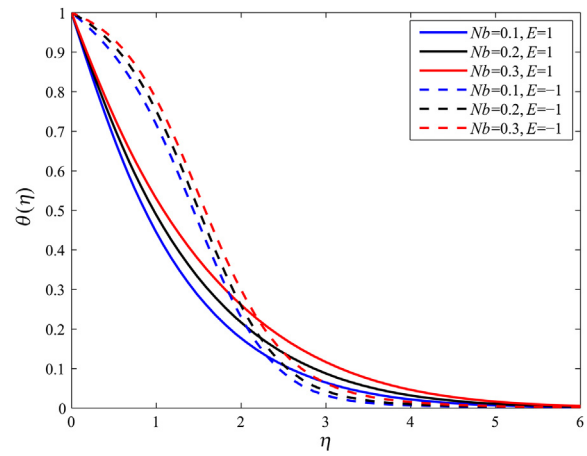


**Figure 8** Variation of fluid temperature with parameters  $Nb$  and  $E$ .

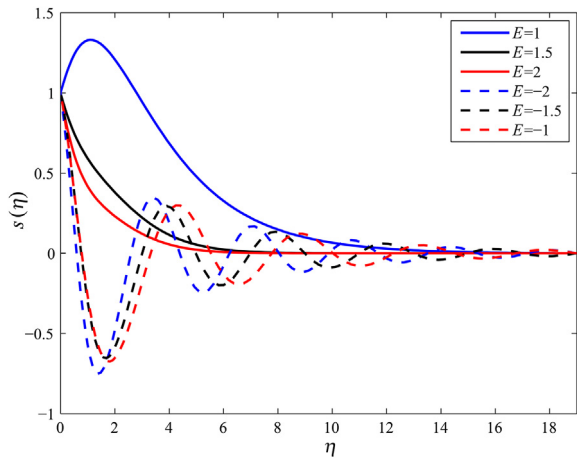


**Figure 7** Variation of fluid concentration with parameter  $E$ .

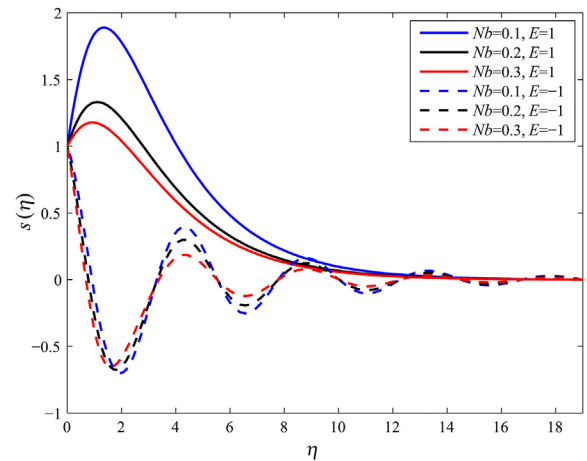


**Figure 9** Variation of fluid concentration with parameters  $Nb$  and  $E$ .

curve for concentration profile is observed for negative values of  $E$ . Arrhenius function decays as activation energy  $E$  enlarges. This eventually promotes the generative chemical reaction due to which temperature rises and concentration declines.

**Figure 8** and **Figure 9** show the temperature and concentration profiles for disparate values of parameter  $Nb$  and two cases of  $E$  (already discussed before). Parameter  $Nb$  has tendency to increase temperature for both values of  $E$  and it reduces concentration for positive  $E$  values.  $Nb$  parameter relates with Brownian motion phenomenon and the Brownian motion is defined as the uncontrolled or erratic movement of particles in a fluid due to their constant collision with other fast-moving molecules. Obviously, due to collision of nanoparticles, heat generates and hence increment in temperature is

found. A similar interpretation is true for concentration that means species between nanoparticles are reduced due to frequent collisions of nanoparticles. Likewise, the previous discussion, wavy concentration curves are obtained for negative  $E$  values.

**Figure 10** and **Figure 11** are displayed to observe the changes in temperature and concentration of fluid with parameter  $Nt$  and two cases of  $E$  values. The augmentation in the temperature is found with  $Nt$  for both values of  $E$ . Apart from it, the boundary layer is thicker for  $E = 1$  than that of  $E = -1$ . The parameter  $Nt$  relates to thermophoresis phenomenon observed in fluid particles where the different particle types exhibit different responses to the force of a temperature gradient. Therefore, increment in  $Nt$ , leads to transport thermal energy due to diffusion of nanoparticles caused by thermophoretic effect and hence the temperature rises. The behaviour of

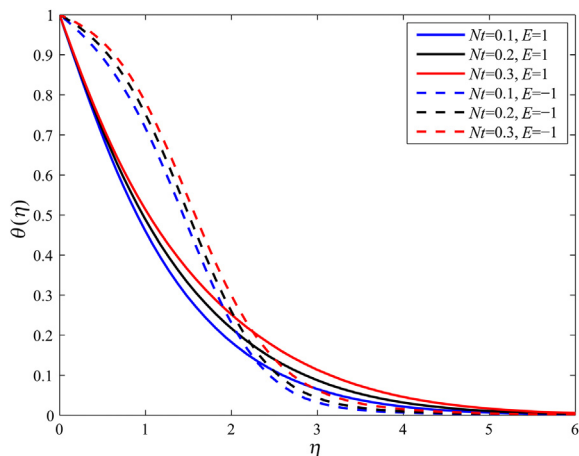


Figure 10 Variation of fluid temperature with parameters  $Nt$  and  $E$ .

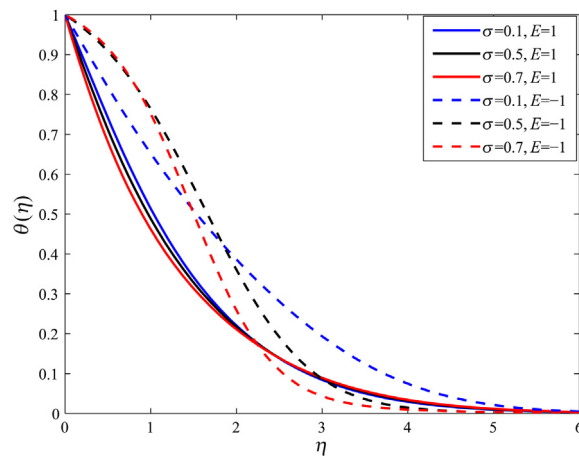


Figure 12 Variation of fluid temperature with parameters  $\sigma$  and  $E$ .

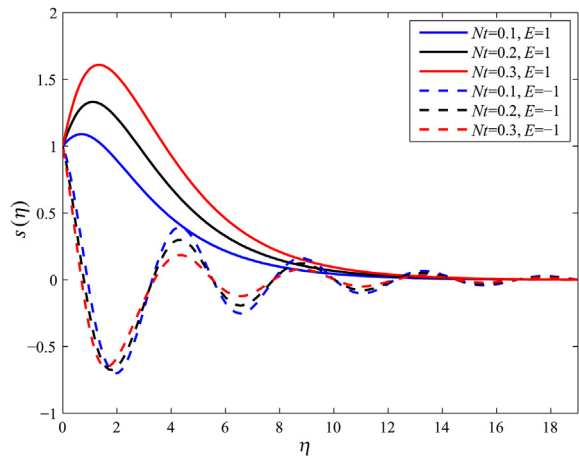


Figure 11 Variation of fluid concentration with parameters  $Nt$  and  $E$ .

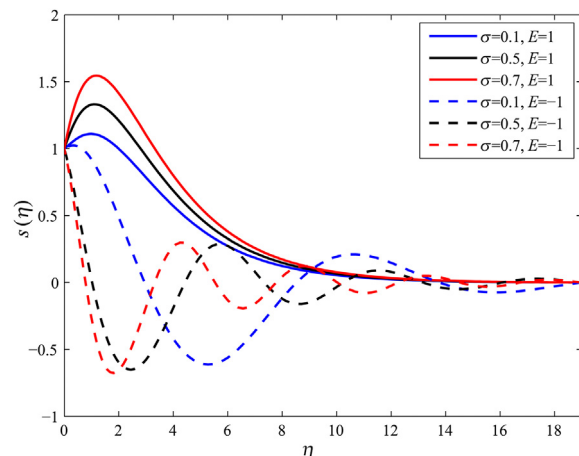


Figure 13 Variation of fluid concentration with parameters  $\sigma$  and  $E$ .

concentration for negative  $E$  values is exactly same as noticed in the previous figure. The concentration profile is enhanced with  $Nt$  for  $E=1$  because thermophoretic phenomena leads to weakening the transport of nanoparticles near the sheet.

The fluid temperature and concentration variation with the change in parameter  $\sigma$  is displayed in Figures 12 and 13. Destructive chemical reaction  $\sigma > 0$  is taken into account. It is observed that for  $E = 1$ , initially, concentration decreases up to  $\eta = 2.5$  but as going away from the surface, concentration starts increasing. Similar dual nature but the exactly opposite tendency is observed for  $E = -1$ . Concentration profile magnifies with  $\sigma$  for  $E = 1$ , and the wavy profile is found for  $E = -1$ , which shows multiple

zeroes of concentration function. Chemical reaction increases the rate of intermolecular mass transfer that causes the volumetric reduction in nanoparticles.

Figure 14 shows the bar diagrams of the values of skin friction coefficient, Nusselt number and Sherwood number for some parameters. It is observed from the bar diagram and Table 2 that skin friction varies with parameter  $A$  and it remains almost same for the rest of the parameters discussed. Increment in  $Nt$  causes reduction in heat transfer. Same behaviour of parameter  $Nt$  is observed by Eid et al. [31]. With rise in parameter  $A$  from 0 to 1 (keeping  $E = 1$ ), skin friction and Sherwood number are increased by 9.36% and 19% respectively, however, Nusselt number is decreased by 26%. For  $E = -1$ , 9.36% and 112%

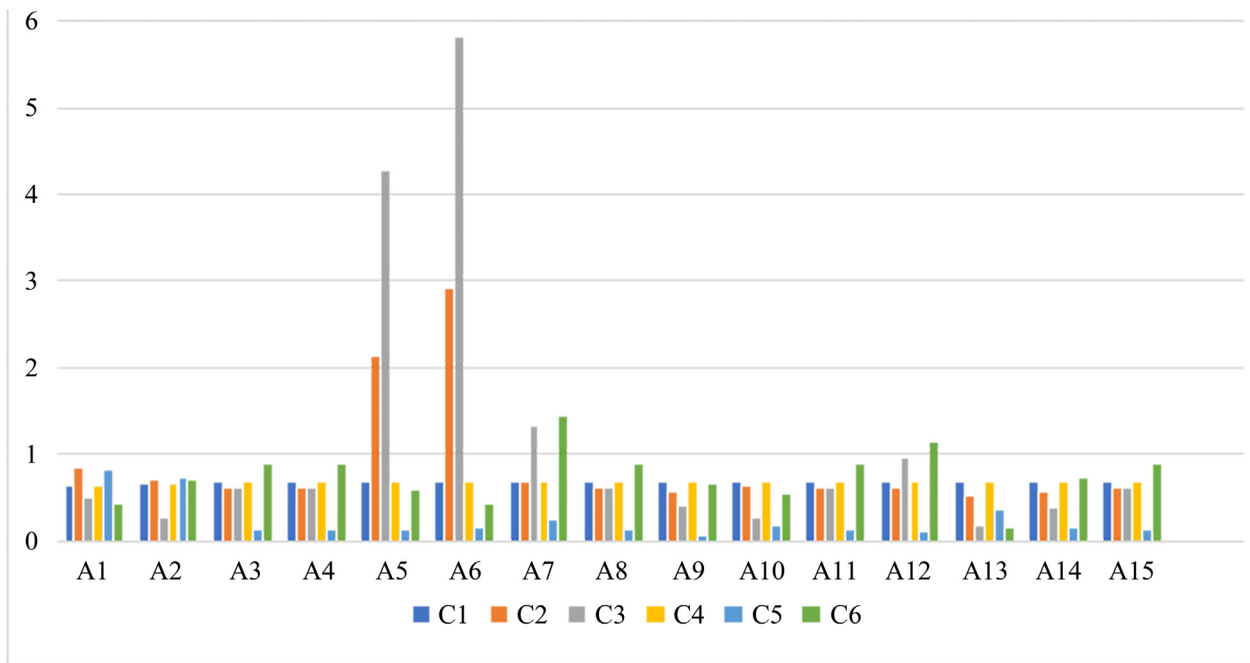


Figure 14 Chart of skin friction, Nusselt number, Sherwood number.

enhancement is observed in skin friction and Sherwood number respectively. For negative activation energy, when  $Nb$  goes from 0.1 to 0.3, heat transfer and mass transfer are reduced by 74% and 54% respectively, however in case of positive activation energy, Nusselt number and Sherwood number decline by 17.18% and 70% respectively. Table 3 represents the standard deviation and standard error in skin friction, Sherwood number and Nusselt number. It is observed that standard deviation is highest for Sherwood

number when  $E=1$  and minimum for skin friction at the surface of sheet.

### 6. Regression analysis for sherwood number

In this section, a quadratic multiple regression method is used to perform statistical analysis for Sherwood number. Regression analysis is used to estimate the relationship between a dependent variable and one or more independent

Table 2 Values of skin friction, Sherwood number and Nusselt number.

	C1	C2	C3	C4	C5	C6
A1	0.6136468	0.82508	0.4964422	0.6136468	0.8035265	0.4114431
A2	0.6433485	0.6845443	0.2605014	0.6433485	0.7066579	0.7036566
A3	0.6710728	0.6105029	0.5948507	0.6710728	0.1162751	0.8747006
A4	0.6710728	0.6105029	0.5948507	0.6710728	0.1162751	0.8747006
A5	0.6710728	2.1212835	4.263745	0.6710728	0.1254667	0.5825484
A6	0.6710728	2.9143537	5.8023196	0.6710728	0.1299129	0.4219999
A7	0.6710728	0.6761092	1.3122313	0.6710728	0.2211434	1.4265288
A8	0.6710728	0.6105029	0.5948507	0.6710728	0.1162751	0.8747006
A9	0.6710728	0.5599369	0.3869381	0.6710728	0.0555529	0.6554148
A10	0.6710728	0.6334014	0.2536008	0.6710728	0.1699305	0.5244172
A11	0.6710728	0.6105029	0.5948507	0.6710728	0.1162751	0.8747006
A12	0.6710728	0.5982996	0.9475628	0.6710728	0.085539	1.1331264
A13	0.6710728	0.4992724	0.1596313	0.6710728	0.3580284	0.135684
A14	0.6710728	0.5486588	0.3620552	0.6710728	0.1397248	0.7184347
A15	0.6710728	0.6105029	0.5948507	0.6710728	0.1162751	0.8747006

[C1 =  $(f''(0), \text{ for } E = 1)$ , C2 =  $(-\theta'(0), \text{ for } E = 1)$ ,  
 C3 =  $(-s'(0), \text{ for } E = 1)$ , C4 =  $(f''(0), \text{ for } E = -1)$ ,  
 C5 =  $(-\theta'(0), \text{ for } E = -1)$ , C6 =  $(-s'(0), \text{ for } E = -1)$ ,  
 A1 =  $(A = 0)$ , A2 =  $(A = 0.5)$ , A3 =  $(A = 1)$ ,  
 A4 =  $(\delta = 0.1)$ , A5 =  $(\delta = 0.5)$ , A6 =  $(\delta = 0.7)$ ,  
 A7 =  $(Nb = 0.1)$ , A8 =  $(Nb = 0.2)$ , A9 =  $(Nb = 0.3)$ ,  
 A10 =  $(Nt = 0.1)$ , A11 =  $(Nt = 0.2)$ , A12 =  $(Nt = 0.3)$ ,  
 A13 =  $(\sigma = 0.1)$ , A14 =  $(\sigma = 0.3)$ , A15 =  $(\sigma = 0.5)$ .]

**Table 3** Standard deviation and standard error in skin friction, Nusselt number and Sherwood number.

	Statistic	Minimum		Maximum		Mean		Std. deviation
		Statistic	Statistic	Statistic	Statistic	Statistic	Std. error	Statistic
C1	15	0.61	0.67	0.6654	0.00413	0.01600		
C2	15	0.50	2.91	0.8742	0.17758	0.68776		
C3	15	0.16	5.80	1.1480	0.02062	1.6290		
C4	15	0.61	0.67	0.6654	0.00413	0.01600		
C5	15	0.06	0.80	0.2251	0.05859	0.22692		
C6	15	0.14	1.43	0.7391	0.08080	0.31294		

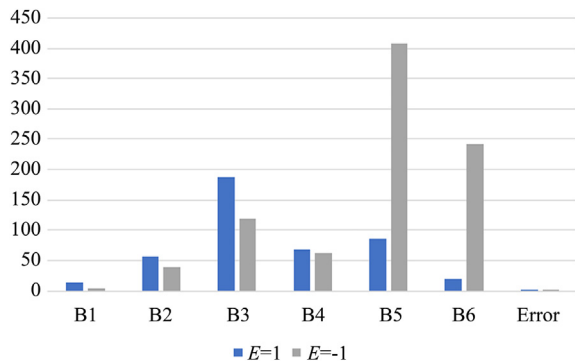


**Figure 15** Chart of regression coefficients.

**Table 4** Values of regression coefficients and error.

	B1	B2	B3	B4	B4	B6	Error
$E = 1$	14.365	56.4686	186.42	68.685	85.635	19.296	0.0019
$E = -1$	3.8233	38.3798	119.78	62.812	407.77	241.41	0.056

variables. This technique is widely applied to predict the outputs, forecasting the data, and finding the causal effect dependencies between the variables. We have taken two fixed values of  $E$  (1 and  $-1$ ), and the value of  $Nb$  and  $Nt$  are generated randomly from the set of 100 values chosen from interval  $[0.1, 0.5]$ . This analysis will suggest us that which parameter has dominant effect on Sherwood number out of  $Nb$  and  $Nt$ . The approximated quadratic regression model is given as follows:

$$Sh_{est} = B1 + B2Nb + B3Nt + B4Nb^2 + B5Nt^2 + B6NbNt$$

where  $Sh_{est}$  is the estimated Sherwood number. The regression coefficients and maximum relative error in this estimation are given in bar diagram Figure 15 and Table 4. It shows that regression coefficient of  $Nt$  is greater than the coefficient of  $Nb$  for both values of activation energy. It reflects that  $Nt$  plays a dominant role than that of  $Nb$  to judge the Sherwood number. It is also noticed that this perturbation of  $Nt$  is lower for negative activation energy.

### 7. Conclusion

We have extensively analysed the impact of flow controlling parameters on MHD stagnation point flow of nano-fluid over a slippery surface in a porous regime by taking both positive and negative values of activation energy. In future, the researchers can explore the effect of negative activation energy on MHD flows by taking many other fluids and boundary constraints. The results are summarized below.

- By managing activation energy negative, the free stream concentration could be achieved at some points within the boundary layer. That means at some points within the boundary layer, the concentration function will behave exactly as it behaves in the ideal fluid. However, the negative activation energy is scarce and assumed in some special cases. Still, the result is beneficial and could also be generalised by using fractional derivatives and fuzzy theory in future studies.
- The temperature goes up with enhancement in  $E$ . Also, the behaviour is identical for both positive and negative values of  $E$ .
- With the rise in parameter  $A$  from 0 to 1 (keeping  $E = 1$ ), skin friction and Sherwood number are increased by 9.36% and 19% respectively, however, Nusselt number is decreased by 26%. For  $E = -1$ , 9.36% and 112% enhancement is observed in skin friction and Sherwood number, respectively.
- For negative activation energy, when  $Nb$  goes from 0.1 to 0.3, heat transfer and mass transfer are reduced by 74% and 54% respectively, however in case of positive activation energy, Nusselt number and Sherwood number decline by 17.18% and 70% respectively.
- Due to the uncontrolled or erratic movement of particles in a fluid, heat generates and hence increment in the temperature is found with augmentation in the parameter  $Nb$ . The wavy concentration curves are found for negative  $E$  values.
- The increment in  $Nt$  leads to transport thermal energy due to diffusion of nanoparticles caused by thermophoretic effect and hence the temperature rises. The concentration profile is enhanced with  $Nt$  for  $E = 1$ .
- For the destructive chemical reaction and  $E = 1$ , initially the concentration decreases up to  $\eta = 2.5$ , but as going away from the surface, the concentration starts

increasing. Similar dual nature but exactly opposite tendency is observed for  $E = -1$ .

- The regression analysis predicts that the regression coefficient of  $Nt$  is greater than that of regression coefficient of  $Nb$  for both values of activation energy ( $E = 1$  and  $-1$ ). It reflects that  $Nt$  plays a dominant role than  $Nb$  to judge the Sherwood number. It is also noticed that the perturbation of  $Nt$  is lower for negative activation energy.

## Acknowledgement

This work is supported by the DST-FIST (Govt. of India) for the grant SR/FIST/MS-1/2017/13.

## References

- [1] G.S. Seth, M.K. Mishra, R. Tripathi, Modeling and analysis of mixed convection stagnation point flow of nanofluid towards a stretching surface: OHAM and FEM approach, *Comput. Appl. Math.* 37 (4) (2018) 4081–4103.
- [2] T.G. Motsumi, O.D. Makinde, Effects of thermal radiation and viscous dissipation on boundary layer flow of nanofluids over a permeable moving flat plate, *Phys. Scripta* 86 (4) (2012) 045003.
- [3] S. Rashidi, S. Akar, M. Bovand, R. Ellahi, Volume of fluid model to simulate the nanofluid flow and entropy generation in a single slope solar still, *Renew. Energy* 115 (2018) 400–410.
- [4] M. Sheikholeslami, S.A. Farshad, Nanoparticles transportation with turbulent regime through a solar collector with helical tapes, *Adv. Powder Technol.* 33 (2022) 103510.
- [5] M. Sheikholeslami, M. Jafaryar, M.B. Gerdroodbary, A.H. Alavi, Influence of novel turbulator on efficiency of solar collector system, *Environ. Technol. Innovat.* 26 (2022) 102383.
- [6] M. Sheikholeslami, Numerical investigation of solar system equipped with innovative turbulator and hybrid nanofluid, *Sol. Energy Mater. Sol. Cells* 243 (2022) 111786.
- [7] M. Sheikholeslami, Numerical analysis of solar energy storage within a double pipe utilizing nanoparticles for expedition of melting, *Sol. Energy Mater. Sol. Cells* 245 (2022) 111856.
- [8] M.E. Haque, M.S. Hossain, H.M. Ali, Laminar forced convection heat transfer of nanofluids inside non circular ducts: a review, *Powder Technol.* 378 (2021) 808–830.
- [9] M.R. Ebrahimmataj, A.E. Tiji, M. Eisapour, H.M. Ali, P. Talebizadehsardari, M.A. Ehteram, S. Abdol maleki, The effect of soot accumulation and backpressure of an integrated after-treatment system on diesel engine performance, *J. Therm. Anal. Calorim.* 147 (2022) 8435–8443.
- [10] F. Hadi, H.M. Ali, Experimental thermal and hydraulic study of super hydrophobic wavy mini channel heat sink using aqueous nanofluids, *Chem. Eng. Commun.* (2021), <https://doi.org/10.1080/00986445.2021.2001459>.
- [11] S. Purree, M. Nadeem, A. Shahzad, H.M. Ali, Synthesis, heat transfer properties and stability of nanofluids for commercialization: a review, *Chem. Eng. Commun.* (2021), <https://doi.org/10.1080/00986445.2021.1976163>.
- [12] W. Ibrahim, A. Dessale, D. Gamachu, Analysis of flow of visco-elastic nanofluid with third order slips flow condition, Cattaneo-Christov heat and mass diffusion model, *Propulsion and Power Research* 10 (2) (2021) 180–193.
- [13] B. Mliki, M.A. Abbassi, Entropy generation of MHD natural convection heat transfer in a heated incinerator using hybrid-nanoliquid, *Propulsion and Power Research* 10 (2021) 143–154.
- [14] S. Arrhenius, Über die Dissociationswärme und den Einfluss der Temperatur auf den Dissociationsgrad der Elektrolyte, *Z. Phys. Chem.* 4 (1889) 96–116.
- [15] M. Javed, A.A. Alderremy, M. Farooq, A. Anjum, S. Ahmad, M.Y. Malik, Analysis of activation energy and melting heat transfer in MHD flow with chemical reaction, *Eur. Phys. J. Plus* 134 (6) (2019) 256.
- [16] A. Majeed, A. Zeeshan, N. Amin, N. Ijaz, T. Saeed, Thermal analysis of radiative bioconvection magnetohydrodynamic flow comprising gyrotactic microorganism with activation energy, *J. Therm. Anal. Calorim.* 143 (3) (2021) 2545–2556.
- [17] N. Saleem, S. Munawar, D. Tripathi, Thermal analysis of double diffusive electrokinetic thermally radiated  $TiO_2$ -Ag/blood stream triggered by synthetic cilia under buoyancy forces and activation energy, *Phys. Scripta* 96 (2021) 095218.
- [18] R. Meenakumari, P. Lakshminarayana, K. Vajravelu, Unsteady MHD flow of a Williamson nanofluid on a permeable stretching surface with radiation and chemical reaction effects, *Eur. Phys. J. Spec. Top.* 230 (5) (2021) 1355–1370.
- [19] B. Nagaraja, B.J. Gireesha, Exponential space dependent heat generation impact on MHD convective flow of Casson fluid over a curved stretching sheet with chemical reaction, *J. Therm. Anal. Calorim.* 143 (2021) 4071–4079.
- [20] M.V. Krishna, Radiation-absorption, chemical reaction, Hall and ion slip impacts on magnetohydrodynamic free convective flow over semi-infinite moving absorbent surface, *Chin. J. Chem. Eng.* (2021), <https://doi.org/10.1016/j.cjche.2020.12.026>.
- [21] L.E. Revell, B.E. Williamson, Why are some reactions slower at higher temperatures? *J. Chem. Educ.* 90 (8) (2013) 1024–1027.
- [22] G.K. Batchelor, *An Introduction to Fluid Dynamics*, Cambridge University Press, Cambridge, 1988.
- [23] P.A. Davidson, *An Introduction to Magnetohydrodynamics*, Cambridge University Press, New York, 2002.
- [24] J.H. Merkin, I. Pop, Stagnation point flow past a stretching/shrinking sheet driven by Arrhenius kinetics, *Appl. Math. Comput.* 337 (2008) 583–590.
- [25] B. Kumar, G.S. Seth, R. Nandkeolyar, A.J. Chamkha, Outlining the impact of induced magnetic field and thermal radiation on magneto-convection flow of dissipative fluid, *Int. J. Therm. Sci.* 146 (2019) 106101.
- [26] B. Kumar, G.S. Seth, M.K. Singh, A.J. Chamkha, Carbon nanotubes (CNTs)-based flow between two spinning discs with porous medium, Cattaneo-Christov (non-Fourier) model and convective thermal condition, *J. Therm. Anal. Calorim.* 146 (2021) 241–252.
- [27] S.S. Motsa, P. Sibanda, A linearisation method for non-linear singular boundary value problems, *Comput. Math. Appl.* 63 (7) (2012) 1197–1203.
- [28] C. Canuto, M.Y. Hussaini, A. Quarteroni, A. Thomas, *Spectral Methods in Fluid Dynamics*, Springer Science & Business Media, 2012.
- [29] C. Canuto, M.Y. Hussaini, A. Quarteroni, T.A. Zang, Theory of stability and convergence for spectral methods, in: *Spectral Methods in Fluid Dynamics*, Springer, Berlin, Heidelberg, 1988.
- [30] W.A. Khan, I. Pop, Boundary-layer flow of a nanofluid past a stretching sheet, *Int. J. Heat Mass Tran.* 53 (11–12) (2010) 2477–2483.
- [31] M.R. Eid, K.L. Mahny, T. Muhammad, M. Sheikholeslami, Numerical treatment for Carreau nanofluid flow over a porous nonlinear stretching surface, *Results Phys.* 8 (2018) 1185–1193.